Correlations and Semi-Universal Analytic Inversion of the TOV Equation

J. M. Lattimer

EOS Measurements with Next-Generation Gravitational-Wave Detectors
INT-N3AS workshop 24-89W

Seattle, Washington
26 August - 4 September, 2024

Acknowledgements

Funding Support:

DOE - Nuclear Physics

DOE - Toward Exascale Astrophysics of Mergers and Supernovae (TEAMS)

NASA - Neutron Star Interior Composition ExploreR (NICER)

NSF - Neutrinos, Nuclear Astrophysics and Symmetries (PFC - N3AS)

DOE - Nuclear Physics from Multi-Messenger Mergers (NP3M)

Recent Collaborators:

Boyang Sun (Stony Brook), Duncan Brown & Soumi De (Syracuse), Christian Drischler, Madappa Prakash & Tianqi Zhao (Ohio), Sophia Han (TDLI), Sanjay Reddy (INT), Achim Schwenk (Darmstadt), Andrew Steiner (Tennessee) & Ingo Tews (LANL)

Pulsar Timing for PSR J0737-3039

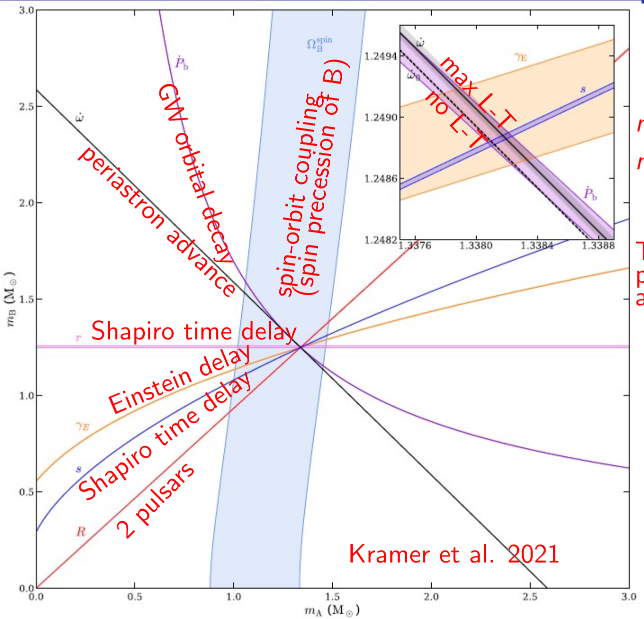

$m_A = 1.338185^{+12}_{-14}\ \mathrm{M}_\odot$

$m_B = 1.248868^{+13}_{-11}\ \mathrm{M}_\odot$

These are the most precisely known masses of any astronomical objects.

Masses of Pulsars in Binaries from Pulsar Timing

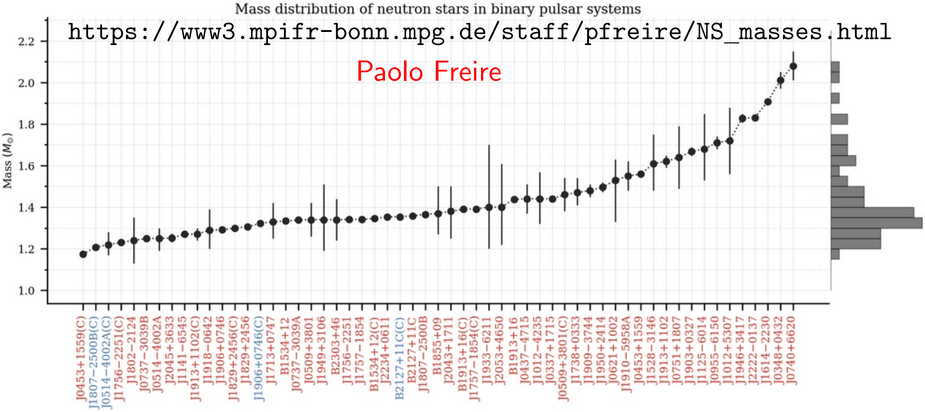

Largest: 2.08 ± 0.07 $M_\odot$
Smallest: 1.174 ± 0.004 $M_\odot$

Several other NS masses have been measured by other means, including some estimated to be more than $2M_\odot$ (e.g., black widow pulsars) and smaller than $1M_\odot$ (HESS J1731-347), but their mass uncertainties are generally large.

How Can a Neutron Star's Radius Be Measured?

- $\text{Flux} = \frac{\text{Luminosity}}{4\pi D^2} = \frac{4\pi R^2 \sigma_B T_s^4}{4\pi D^2} = \left(\frac{R}{D}\right)^2 \sigma_B T_s^4$
  X-ray observations of quiescent neutron stars in low-mass X-ray binaries measure the flux and surface temperature T_s. Distance D somewhat uncertain; GR effects introduce an M dependence.
- $F_{Edd} = \frac{GMc}{\kappa D^2}$ X-ray observations of bursting neutron stars in accreting systems measure the Eddington flux F_{Edd}. κ is the poorly-known opacity; GR effects introduce an R dependence.
- X-ray phase-resolved spectroscopy of millisecond pulsars with nonuniform surface emissions (hot spots). NICER: PSR J0030+0451, PSR J0437-4715 (closest and brightest millisecond pulsar) and PSR J0740+6620 (most massive pulsar).
- $R_{1.4} \simeq (11.5 \pm 0.3) \frac{\mathcal{M}}{M_\odot} \left(\frac{\tilde{\Lambda}}{800}\right)^{1/6} \text{km}, \quad \mathcal{M} = \frac{(M_A M_B)^{3/5}}{(M_A + M_B)^{1/5}}$
  GW observations of neutron star mergers measure the chirp mass $\mathcal{M}$ and binary tidal deformability $\tilde{\Lambda}$ (GW170817).
- $I_A \propto M_A R_A^2$ Radio observations of extremely relativistic binary pulsars measure masses M_A, M_B and moment of inertia I_A from spin-orbit coupling [PSR J0737-3039 ($P_b = 0.102$d), PSR J1757-1854 (0.164 d), PSR J1946+2052 (0.078 d)].

Summary of Astrophysical Observations

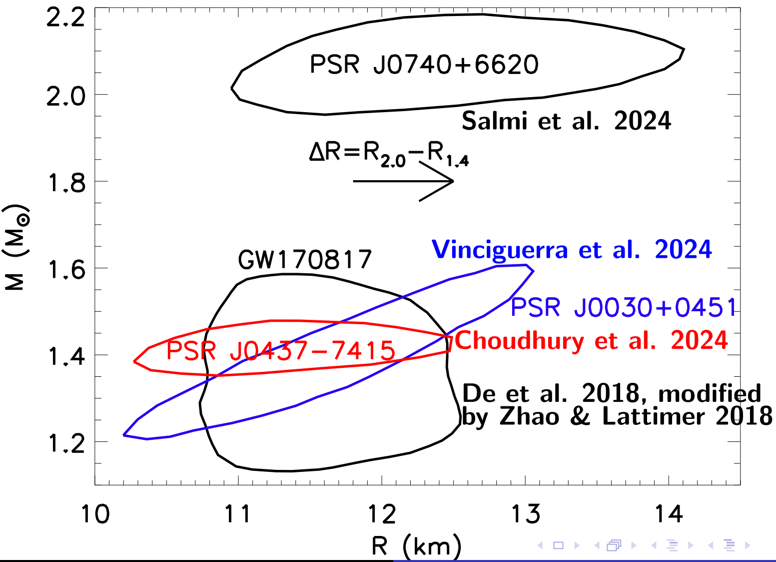

Neutron Star Structure

Tolman-Oppenheimer-Volkov equations

$$\frac{dp}{dr} = -\frac{G}{c^4}\frac{(mc^2+4\pi pr^3)(\varepsilon+p)}{r(r-2Gm/c^2)}$$

$$\frac{dm}{dr} = 4\pi\frac{\varepsilon}{c^2}r^2$$

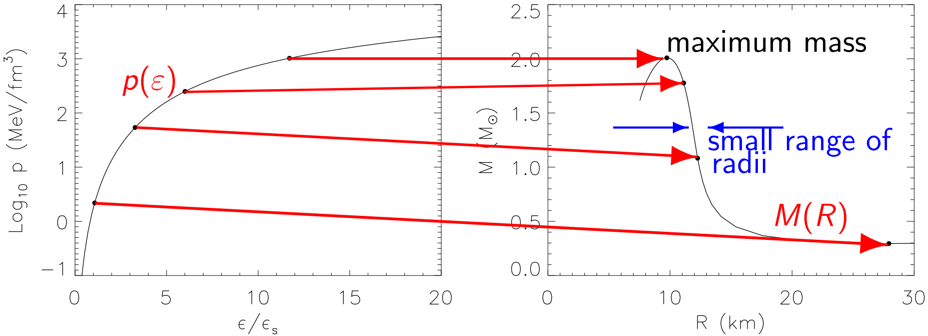

Equation of State ← Observations

The Radius – Pressure Correlation

9.52 ± 0.49

7.06 ± 0.24

5.68 ± 0.14

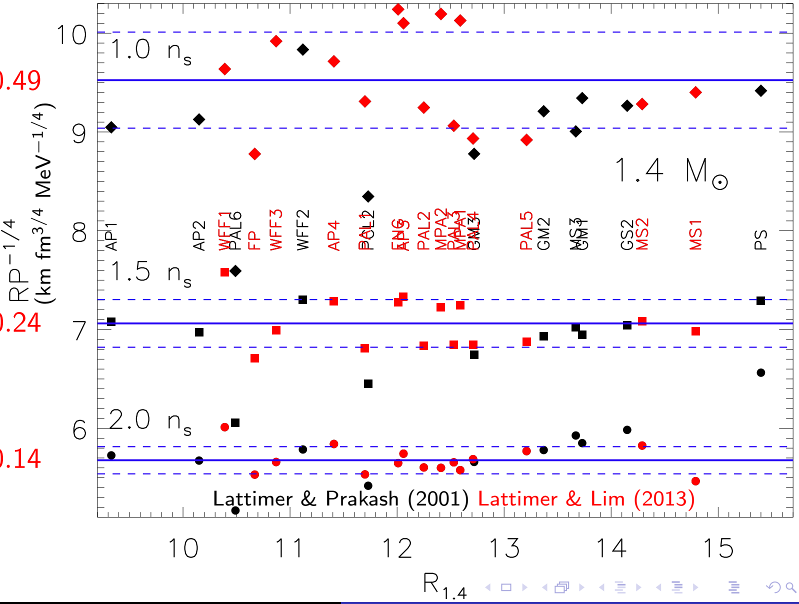

The I-Love Relation

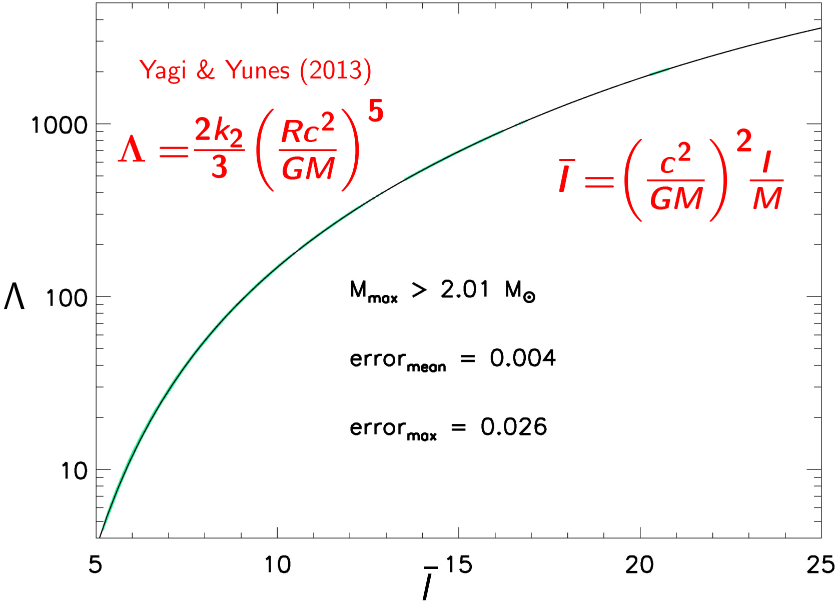

F-Mode Properties - Moment of Inertia

$$\Omega_f = \frac{GM\omega_f}{c^3}$$

Zhao & Lattimer 2022

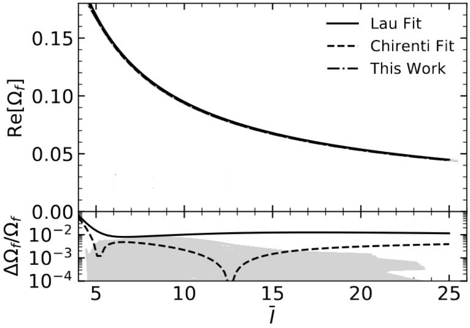

frequency

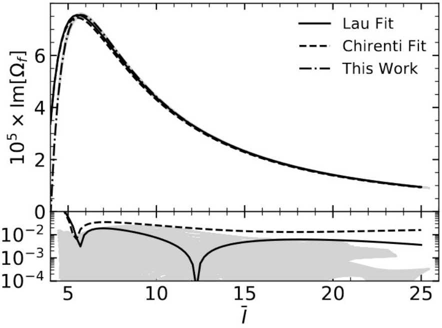

damping time

Neutron Skin Thickness - L

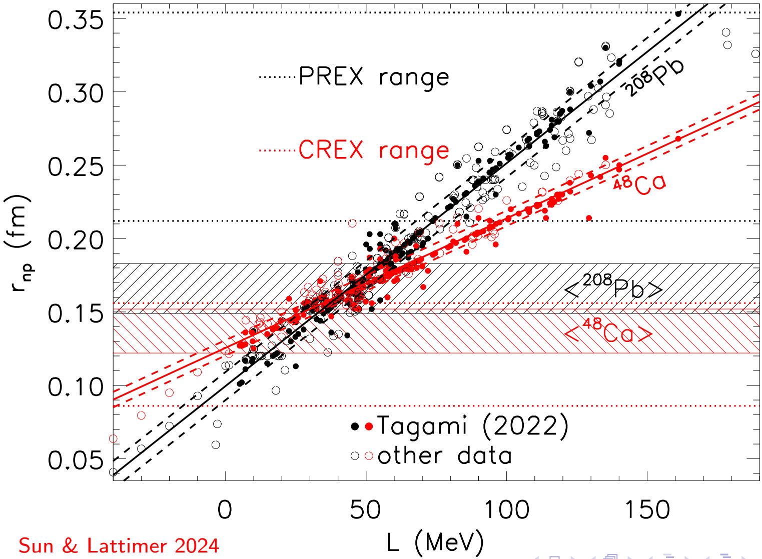

Sun & Lattimer 2024

Maximum Mass As a Unique Scaling Point

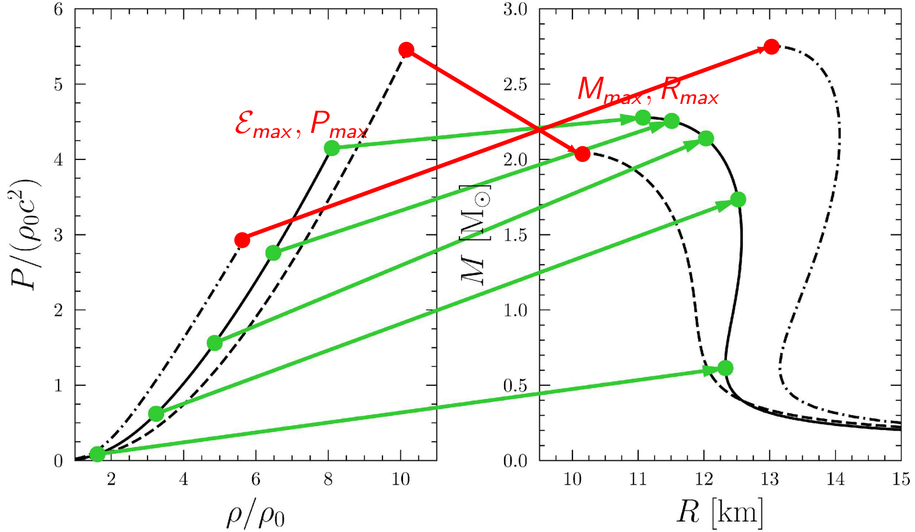

Varying the EOS

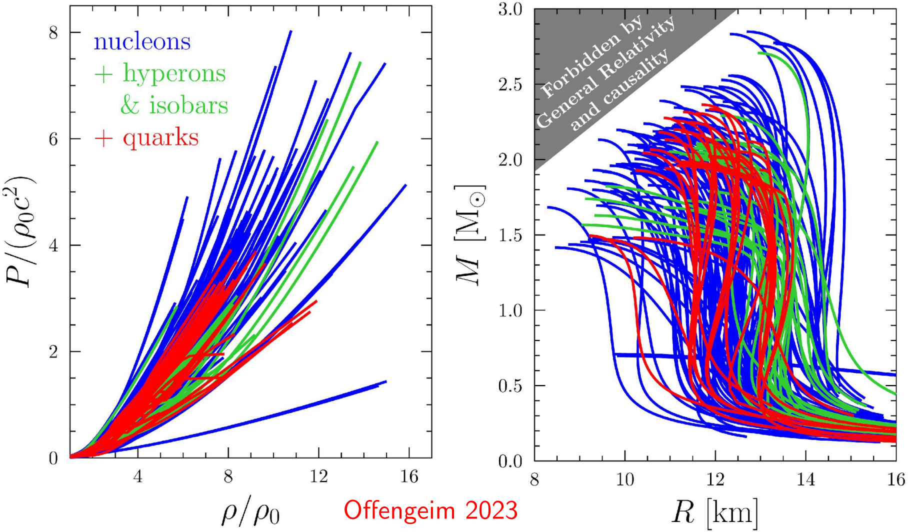

Offengeim 2023

$M_{\max}, R_{\max}, \mathcal{E}_{\max}, P_{\max}$ Correlations

• Ofengeim(2020) fitted $\mathcal{E}_{max}$ and P_{max} with the functions

$$\mathcal{E}_{max}, P_{max} \simeq \left[\frac{a_{\mathcal{E},P}}{R_{max}\cos\phi_{\mathcal{E},P} + (GM_{max}/c^2)\sin\phi_{\mathcal{E},P} + d_{\mathcal{E},P}}\right]^{s_{\mathcal{E},P}}$$

with accuracies of about 3% and 8%, respectively.

• Cai, Li and Zhang (2023) found a perturbative solution of the TOV equations in the parameter $x = P_c/\mathcal{E}_c$:

$$R \simeq \sqrt{\frac{3c^2}{2\pi G\mathcal{E}_c}}\left[\frac{x}{1+4x+3x^2}\right]^{1/2},$$

$$M \simeq \sqrt{\frac{54c^6}{\pi G^3\mathcal{E}_c}}\left[\frac{x}{1+4x+3x^2}\right]^{3/2}.$$

At M_{max}, accuracies are 7% and 8%; at $1.4M_\odot$, they are 2% and 6%.

- Ofengeim et al. (2023) suggested fits for M_{max}, R_{max}:

$$M_{max} \simeq \frac{a_M \mathcal{E}_{max}^{-1/2} x^{3/2}}{b_M + c_M x^{p_M} \mathcal{E}_{max}^{q_M}}, \quad R_{max} \simeq \frac{a_R \mathcal{E}_{max}^{-1/2} x^{1/2}}{b_R + c_R x^{p_R} \mathcal{E}_{max}^{q_R}}$$

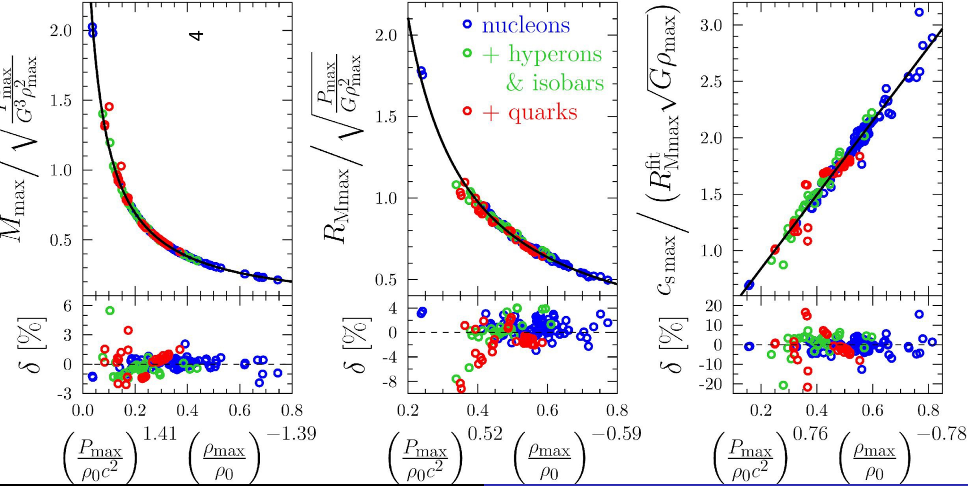

$M_{\max}, R_{\max}, \mathcal{E}_{\max}, P_{\max}$ Correlation

Ofengeim et al's finding suggest the power-law correlations

$$\mathcal{E}_{\rm c,max} = (1.809 \pm 0.36)\left(\frac{R_{\max}}{10{\rm km}}\right)^{-1.98}\left(\frac{M_{\max}}{M_\odot}\right)^{-0.171} {\rm GeV\ fm}^{-3},$$

$$P_{\rm c,max} = (118.5 \pm 6.2)\left(\frac{R_{\max}}{10{\rm km}}\right)^{-5.24}\left(\frac{M_{\max}}{M_\odot}\right)^{2.73} {\rm MeV\ fm}^{-3},$$

which are accurate to about 5% in fitting $\mathcal{E}_{c,max}$ and $P_{c,max}$.

Points along $M-R$ curves, at $M = fM_{\max}$, have similarly accurate correlations:

$$\mathcal{E}_{c,f} = a_{\mathcal{E},f} R_{fM_{max}}^{b_{\mathcal{E},f}} M_{max}^{c_{\mathcal{E},f}}$$

$$P_{c,f} = a_{P,f} R_{fM_{max}}^{b_{P,f}} M_{max}^{c_{P,f}}$$

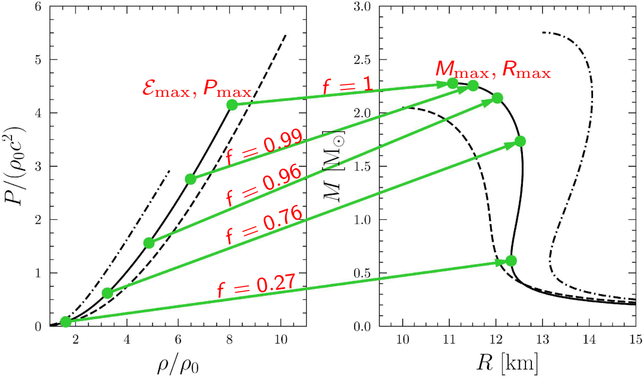

(M, R) Is Not Equivalent To $(\mathcal{E}_c, P_c)$

While the maximum mass point (M_{max}, R_{max}) predicts $(\mathcal{E}_{c,max}, P_{c,max})$ to about 5%, and similarly for a given fractional maximum mass fM_{max}, the inversion is not unique. Two different equations of state predicting the same (M, R) (numbers in figure) arrive at those values from integration via different paths in $(\mathcal{E}, P)$ space. Similarly, two equations of state with identical values of $(\mathcal{E}_c, P_c)$ (letters) do not have the same (M, R) values.

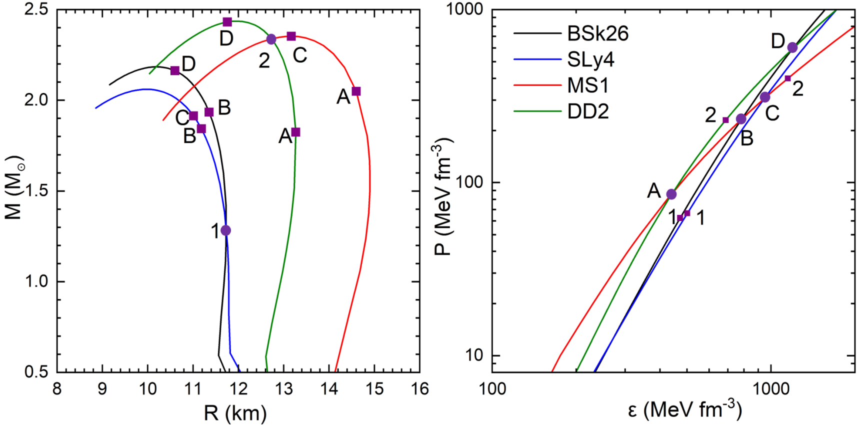

Correlations at $M = fM_{\rm max}$

Thus, more information than (M,R) needed. We find precision is greatly improved using a 2nd radius from a grid of fractional M_{max} points, *e.g.*, $f \in [1, 0.95, 0.9, 0.85, 4/5, 3/4, 2/3, 0.6, 0.5, 0.4, 1/3]$.

$$\mathcal{E}_f = a_{\mathcal{E},f}\left(\frac{R_{f_1}}{10\rm km}\right)^{b_{\mathcal{E},f_1}}\left(\frac{R_{f_2}}{10\rm km}\right)^{c_{\mathcal{E},f_2}}\left(\frac{M_{max}}{M_\odot}\right)^{d_{\mathcal{E},f}},$$
$$P_f = a_{P,f}\left(\frac{R_{f_1}}{10\rm km}\right)^{b_{P,f_1}}\left(\frac{R_{f_2}}{10\rm km}\right)^{c_{P,f_2}}\left(\frac{M_{max}}{M_\odot}\right)^{d_{P,f}},$$

$f = M/M_{\rm max}$	f_1	f_2	$\Delta(\ln \mathcal{E}_f)$	f_1	f_2	$\Delta(\ln P_f)$
1	0.95	0.9	0.00469	1	3/5	0.0123
0.95	0.95	4/5	0.00275	0.95	3/5	0.00722
0.90	0.95	2/3	0.00227	0.95	2/5	0.00517
0.85	0.95	1/2	0.00237	0.9	2/5	0.00491
4/5	0.9	1/2	0.00230	0.85	2/5	0.00463
3/4	0.85	1/2	0.00239	4/5	2/5	0.00539
2/3	3/4	1/2	0.00277	2/3	2/5	0.00513
3/5	3/4	2/5	0.00339	2/3	1/3	0.0172
1/2	2/3	1/3	0.00477	1/2	2/5	0.00996
2/5	1/2	1/3	0.00706	1/2	1/3	0.0187
1/3	1/2	1/3	0.0122	2/5	1/3	0.0259

greatly reduced uncertaintites!

Testing the Inversion

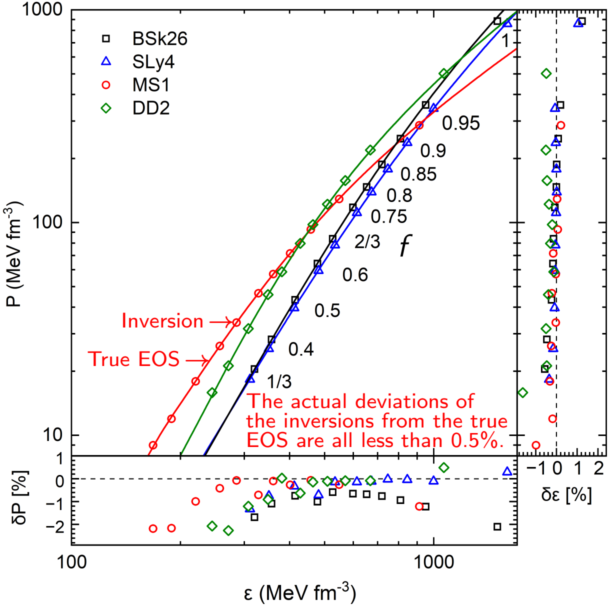

Testing the Inversion for $c_s^2 - P/\mathcal{E}$

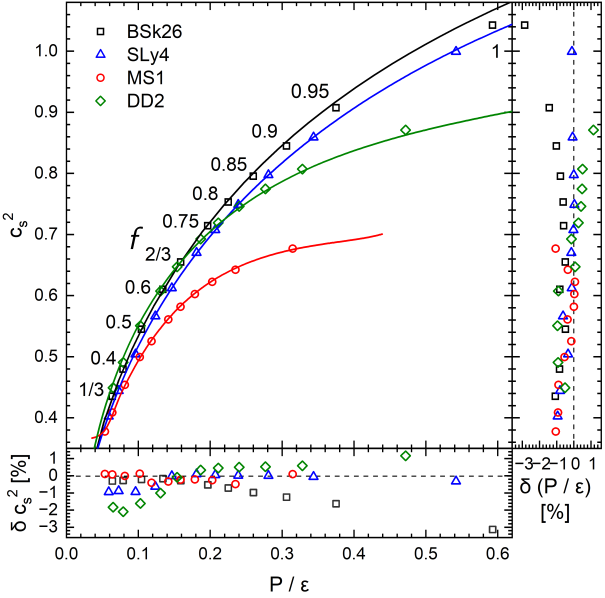

Comparing Inversions

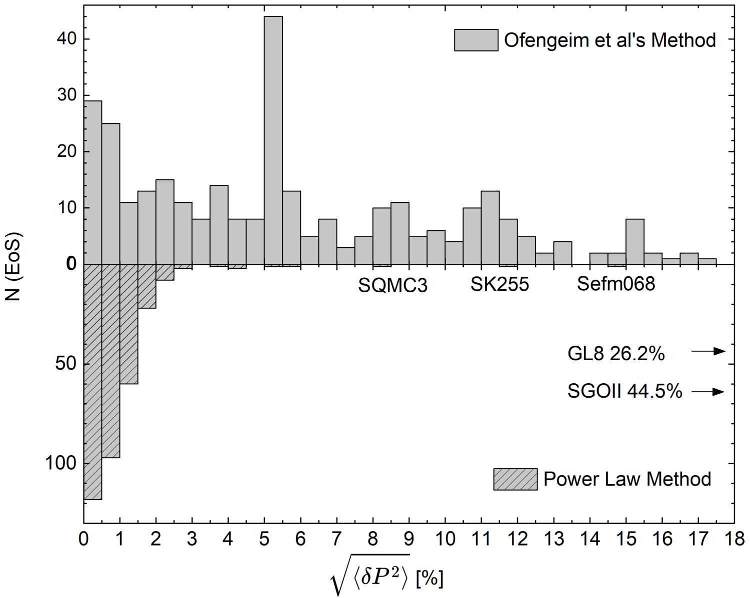

Inversion of $M - R$ Data

Instead of inverting an $M - R$ curve one may wish to infer the EOS from $M - R$ data. Traditional Bayesian inversions begin with $M - R$ priors generated by sampling millions of trials using a specific EOS parameterization with uniform distributions of parameters within selected ranges.

One problem with our approach is that M_{max} and R_{max} are not known. One can form analytical correlations between (M, R) and $(\mathcal{E}_c, P_c)$, but these have only moderate accuracy since this inversion is not unique. More information than the $M - R$ point itself is necessary to improve the inversion.

One possibility is to include the inverse slope dR/dM at the (M, R) point. Generally, one can determine a correlation between a quantity $G \in [\mathcal{E}_c, P_c, \mathrm{etc.}]$ and $(M, R, dR/dM)$ in the form

$$\ln G = \ln a_G + b_G \ln M + c_G \ln R + d_G(dR/dM).$$

Including dR/dM information improves correlations by factors of about 2. It is also found that inferred values of $\mathcal{E}_c$ and P_c are highly correlated; fits to $P_c/\mathcal{E}_c$ have much smaller uncertainty than fits to $\mathcal{E}_c$ or P_c.

Testing the $M - R$ Inversion

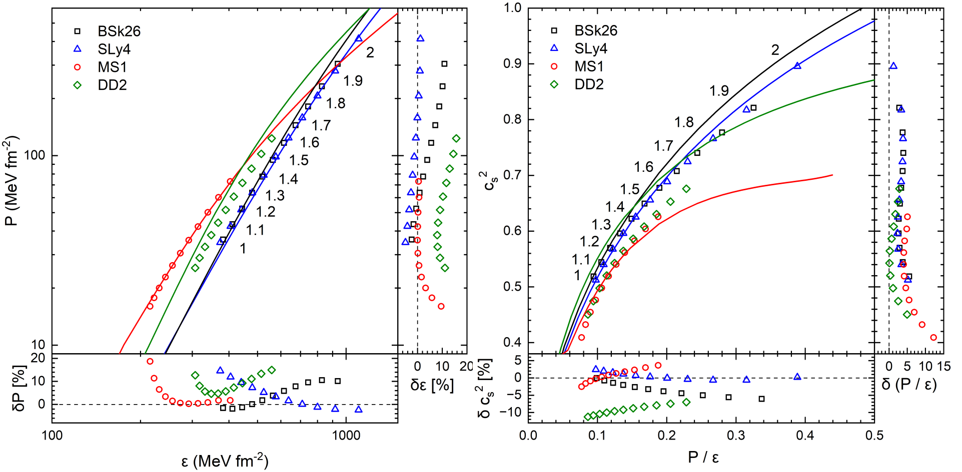

Comparison to Traditional Bayesian Inference

From two $M - R$ regions obtained from observations select random pairs of points and determine dR/dM. Then, using the above correlation formulae, infer two $\mathcal{E}_c - P_c$ uncertainty regions (after rejecting pairs that violate the conditions $0 \leq dP_c/d\mathcal{E}_c \leq 1$ and $dP_c/dM > 0$).

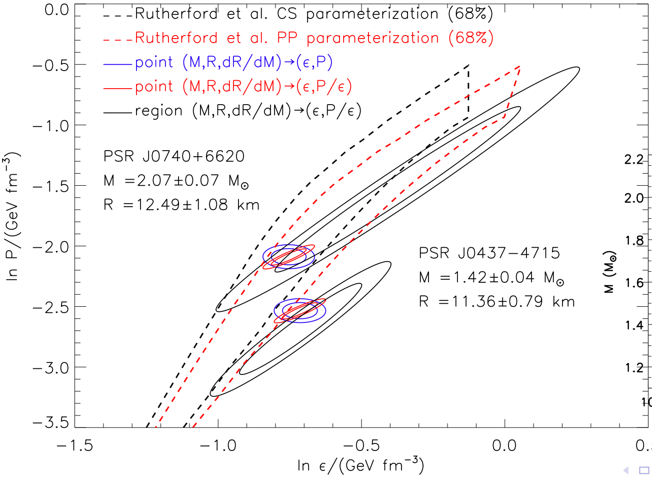

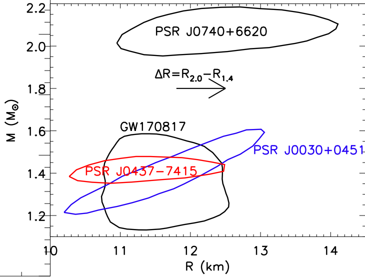

Importance of $\Delta R = R_{2.0} - R_{1.4}$

- J0437-4715: $R = 11.36^{+0.95}_{-0.63}$ km
- J0740+6620: $R = 12.49^{+1.28}_{-0.88}$ km

$\Delta R = +1.13^{+1.59}_{-1.08}$ km

313 Skyrme + RMF forces with $M_{max} \geq 2.0 M_\odot$

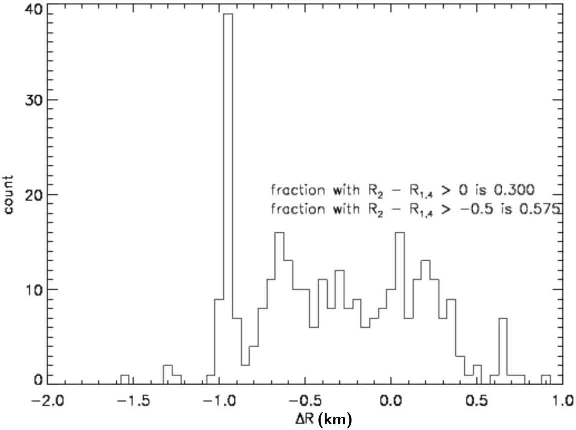

Applications

- Analytic inversion of TOV equations with arbitrarily high accuracies (depends on number of R_f values).
- Existing techniques use parameterized EOS models in probabilistic (Bayesian) approaches having unquantified systematic uncertainties stemming from the model and parameter choices (prior distributions).

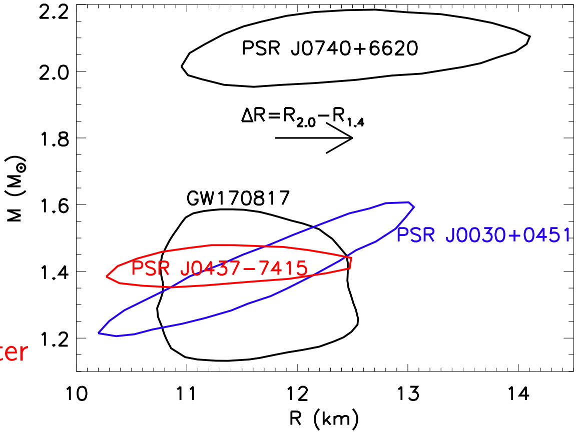

- Since M and R can't uniquely determine $\mathcal{E}_c$ and P_c, we use the value of (dR/dM) to improve accuracies.
- Correlations of c_s with M, R and dR/dM can be used to further improve the fidelity of inversions and also for interpolating within the $\mathcal{E}_f - P_f$ grid. They could also allow probing the composition of the neutron star interior (phase transitions, etc.).
- Correlations of $\tilde{\Lambda}, \bar{I}$ and BE$/M$ with M and R also exist and aren't sensitive to dR/dM.
- This inversion technique might have wider applicability to other physics or engineering problems.